^{13}N + p elastic resonance scattering via a thick-target method

Y. B. Wang, B. X. Wang, X. Qin, X. X. Bai, B. Guo, C. Jiang, Y. J. Li, Z. H. Li, G. Lian, J. Su, S. Zeng, and W. P. Liu

China Institute of Atomic Energy, P. O. Box 275(46), Beijing 102413, People's Republic of China

(Received 26 September 2007; revised manuscript received 15 January 2008; published 10 April 2008)

The ^{13}N + p elastic resonance scattering has been studied in inverse kinematics via a thick-target method. A ^{13}N secondary beam of 47.8 ± 1.5 MeV produced by the ^{2}H(^{12}C,^{13}N)n reaction was used to bombard a 9.33 mg/cm^2 $(CH_2)_n$ target. The recoil protons were detected by a ΔE-E silicon counter telescope at $\theta_{lab} = 15^\circ$. The performance of the setup was checked by ^{12}C + p elastic resonance scattering with the same $(CH_2)_n$ target. The excitation function for the ^{13}N(p, p) elastic scattering was obtained in the energy interval of $E_{c.m.} \sim 0.5$–3.2 MeV and was analyzed by using a multilevel R-matrix code MULTI7. Several low-lying excited states in ^{14}O were surveyed. Our results confirm a very recent 2^- assignment to the 6.8 MeV level and agree with the observation of a new 0^- level at 5.7 MeV with a width of 400(45) keV.

DOI: 10.1103/PhysRevC.77.044304 PACS number(s): 21.10.Hw, 21.10.Jx, 25.40.Ny, 27.20.+n

I. INTRODUCTION

The properties of low-lying levels close to the proton threshold in light exotic nuclei are crucial in nucleosynthesis of astrophysical proton capture and of nuclear structure significance. For this purpose, the excitation function of proton elastic scattering is usually employed to explore the levels and resonance parameters, i.e., J^π, Γ_p, etc. To use a radioactive secondary beam of relatively low intensity, a thick-target method has been recently proposed and rapidly applied [1,2]. It uses either a solid or a gas target containing hydrogen atoms with thickness enough to stop the incident beam and the heavier reaction products. The proton energy spectrum provides the excitation function with an energy interval corresponding to the energy loss of the incident beam. The advantage of this method is that one can obtain the excitation function in a one-shot experiment. Up to now, several light nuclei systems up to ^{21}Na + p have been investigated with this method [3–9].

^{13}N(p, γ)^{14}O is one of the key reactions involved in the hot CNO cycle that takes place in the evolution of massive stars. Its reaction rates are dominated by the 1^- broad resonance state that lies at 5.16 MeV in ^{14}O [10–15]. However, there are several low-lying levels above the ^{13}N + p threshold that might be of relevance to the reaction rates and of importance to the nuclear structure of ^{14}O. The properties of these levels are not well known; in particular, there is a 0^- level missing when comparing with the mirror nucleus ^{14}C [16]. Recently, the charge exchange reaction of ^{14}N(^{3}He, t)^{14}O was studied by A. Negret *et al.* [17], the widths of several known levels were determined. In their work, the width of the 6.3 MeV 3^- level was determined to be 50(6) keV, which differs significantly from the compiled value of 103(6) keV [16]. In the course of the preparation of this article, a similar ^{13}N + p elastic resonance scattering was published [8], in which a clear assignment of 2^- to the 6.8 MeV level in ^{14}O was made for the first time and a new 0^- level at 5.7 MeV with a width of 400(100) keV was suggested. These results are confirmed in the work reported here.

II. EXPERIMENT

The experiment was carried out at the radioactive secondary beam line [18,19] of the HI-13 Tandem accelerator laboratory, Beijing. Recently, a Danfysik Wien velocity filter was installed in the beam line, which brings substantial improvements in the secondary beam quality. Some details concerning the ^{13}N secondary beam and the experimental setup are presented in this section.

A. The secondary beam

The ^{13}N secondary beam was produced via the reaction ^{2}H(^{12}C,^{13}N)n. A 100- to 150-pnA ^{12}C beam of 72 MeV was used to bombard a 4.8-cm-long deuterium gas cell at a pressure of about 1.5 atm. The front and rear windows of the gas cell were Havar foils of 1.9 mg/cm^2 in thickness. After magnetic separation and focus with a dipole and a quadruple doublet, the secondary beam was further purified by the Wien filter and was then collimated by a ϕ9- to ϕ5-mm collimator complex. During the experiment, the intensity of the secondary beam was about 6000–10000 particles/s, and the purity about 82–90%. In addition to the ^{12}C contaminants from multiple scattering of primary ions, there were small amounts of ^{6}Li and ^{4}He in the secondary beam that were due to the ^{2}H(^{12}C,^{6}Li)^{8}Be and ^{2}H(^{12}C,α)^{10}B reactions, respectively. The secondary beam may also contain protons from the ^{2}H(^{12}C,p)^{13}C reaction, these were not detected because of very small energy loss in the detector used in the beam-tuning runs.

B. Experimental setup

A schematic layout of the experimental setup is shown in Fig. 1. The secondary beam was analyzed by a 13.2-μm-thick silicon ΔE detector. The output of this ΔE detector was taken into spectra by a multichannel analyzer to monitor the purity of ^{13}N and was recorded by a scaler for beam normalization. Moreover, it was also included as a parameter to remove

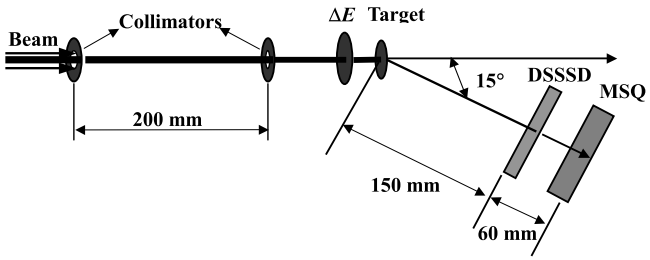

FIG. 1. Schematic layout of the experimental setup for the ^{1}H(^{13}N, p)^{13}N reaction.

proton events generated from ions other than ^{13}N. At the counting rates mentioned above, the spectroscopy amplifier for the 13.2-μm silicon detector generated pulse pile-up of about 5–9%, the pile-up reject output was also recorded by the scaler for correction of the beam losses. In between the collimator complex and the 13.2-μm silicon detector, a set of a ΔE-E telescope of silicon detectors was installed on a movable ladder for beam-tuning and purity cross-check. The energy of the ^{13}N ions impinging on the 9.33 mg/cm^2 thick $(CH_2)_n$ target was about 47.8 $\pm$ 1.5 MeV. A carbon foil of 10.88 mg/cm^2 in thickness was applied to evaluating the background that arose from the carbon atoms in the $(CH_2)_n$ target. Both targets were thick enough to fully stop the ^{13}N ions; however, there were leakages of ^{12}C and light ions like ^{6}Li and ^{4}He, etc.

The recoil protons from the ^{1}H(^{13}N,p)^{13}N reaction were detected by a ΔE-E telescope consisting of a 63-μm-thick Double-Sided Silicon Strip Detector (DSSSD) [20] and a 982-μm-thick quadrant silicon detector (MSQ) [20]. Both detectors are 50 $\times$ 50 mm^2 in size. The DSSSD has a resolution of 3 $\times$ 3 mm^2, defined by the width of microstrips orthogonally oriented on both sides. The ΔE-E telescope was placed at 150 mm downstream from the $(CH_2)_n$ target to compromise the counting rates and resolution. To avoid the direct bombardment of the DSSSD by the leaked ^{12}C and light ion components, the ΔE-E telescope was placed at 15° instead of 0°. In this geometry, the laboratory angle of each pixel of the DSSSD can be evaluated according to the following formula,

$$\theta_{\rm lab} = \arccos\left(\frac{d_0\cos 15^\circ \pm x\sin 15^\circ}{\sqrt{d_0{}^2 + x^2 + y^2}}\right). \qquad (1)$$

In the formula, d_0 refers to the distance between the centers of the target and the DSSSD, and x, y are the coordinates in the plane of the DSSSD if setting the origin at its center. Due to the limitation of the available data acquisition system, only half of the DSSSD area was used while the outer part was blocked. For the inner half thus used, the DSSSD covered about 10°–20° in the laboratory frame, corresponding to 140°–160° in the center of mass frame.

In about 100 h of beam time, runs with the $(CH_2)_n$ and carbon targets were taken at a ratio of 3:1. A calibrated ΔE-E_t spectrum measured with the DSSSD and MSQ detectors is shown in Fig. 2. The calibration was made with proton beam scattering on Au of 440 μg/cm^2 at several energies and with a standard ^{239}Pu-^{241}Am mixed source. To provide a cross-check of the calibration and the performance of the setup, ^{12}C + p

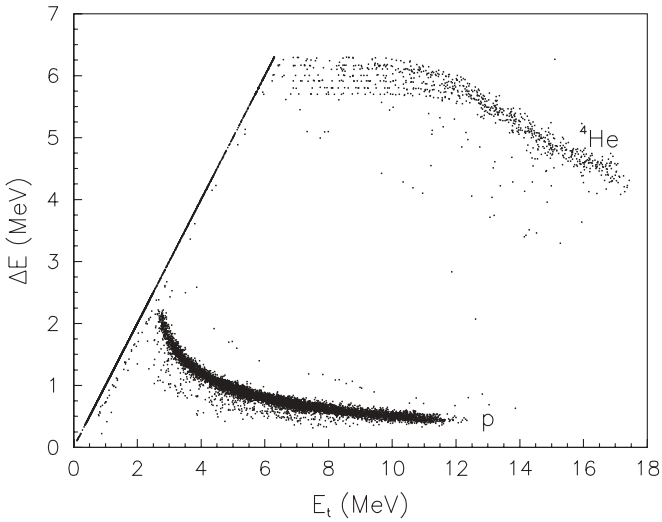

FIG. 2. A calibrated ΔE-E_t spectrum measured with the DSSSD and MSQ detectors. The background spectrum with the carbon target is similar.

elastic resonance scattering was studied successively using the same setup to map the well-known levels in ^{13}N. In the ^{12}C + p runs, the gas cell was pumped empty, the ^{12}C beam initially of 60 MeV was scattered by the Havar foils into the secondary beam line. The ^{12}C ions lost partly their energies in the 13.2-μm silicon detector, impinging on the $(CH_2)_n$ target with an energy of 46.3 $\pm$ 1.1 MeV. The carbon target also served for the background measurement. The intensity of ^{12}C that bombarded the $(CH_2)_n$ target was about 1–2 $\times$ 10^4 pps.

III. ANALYSIS AND RESULTS

A. Data analysis

At the reaction point, the center-of-mass energy $E_{\rm c.m.}$ has a simple relation with the proton energy E_p as the following:

$$E_{\rm c.m.} = E_p \times \frac{m_1 + m_{13}}{4m_{13}\cos^2\theta_{\rm lab}}, \qquad (2)$$

where m_1 and m_{13} are the masses of proton and ^{13}N, respectively, and $\theta_{\rm lab}$ is the laboratory scattering angle. To transform the detected proton total energies E_t into $E_{\rm c.m.}$, one needs to know the energy losses of the protons in the $(CH_2)_n$ target ΔE_p according to each $\theta_{\rm lab}$, this was done with a Monte-Carlo simulation combining the reaction kinematics with the energy losses of ^{13}N and protons. As an example, a simulated ΔE_p versus E_t for a pixel centered at $\theta_{\rm lab} = 10.9^\circ$ is shown in Fig. 3. In the simulation, the ^{13}N beam energy was taken as 47.8 $\pm$ 1.5 MeV and the $\theta_{\rm lab}$ resolution as 2.5°(FWHM), mainly resulting from the beam angular resolution (1.4°) and the beam spot (1.9°). Combining ΔE_p with E_t, the proton energy at the reaction point $E_p = E_t + \Delta E_p$ was obtained that was then converted into $E_{\rm c.m.}$ according to Eq. (2). After the E_p to $E_{\rm c.m.}$ conversion, the proton spectra were added up over different $\theta_{\rm lab}$. In the course of E_p to $E_{\rm c.m.}$ conversion, the uncertainty of $E_{\rm c.m.}$ was estimated to be $\pm$20 keV mainly due

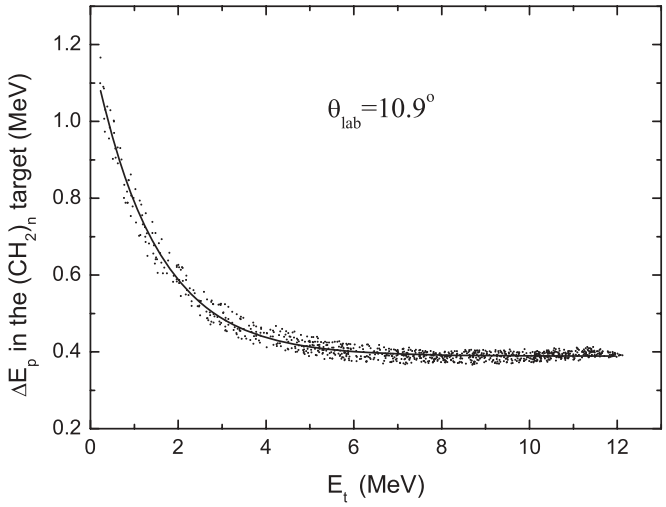

FIG. 3. The simulated proton energy loss in the $(CH_2)_n$ target versus the detected proton total energy for a pixel centered at $\theta_{\rm lab} = 10.9^\circ$. The data were fitted with a first-order exponential decay function to retrieve the proton energy loss in the target.

to the $\theta_{\rm lab}$ resolution and energy straggling of particles in the target.

The background proton yields with the carbon target were normalized to those with the $(CH_2)_n$, by the total number of the ^{13}N ions and by the number of carbon atoms in the effective target thickness related to per $E_{\rm c.m.}$ unit. The latter was done by computing the range difference, i.e., the ^{13}N range difference between the maximum and the minimum energies of per $E_{\rm c.m.}$ unit in the $(CH_2)_n$ and carbon, respectively. After the normalization, the proton yield from the carbon target was about 1/7 of that from the $(CH_2)_n$ target. The net proton yields were then obtained by subtracting the normalized background events of the carbon target.

The net proton yields of $^{13}\mathrm{N} + p$ were converted into the averaged differential cross section according to

$$\frac{dN_p}{dE} = N_{^{13}N}\frac{dN_{\rm target}}{dE}\frac{d\sigma}{d\Omega}d\Omega. \tag{3}$$

In the formula, dN_p/dE refers to the net proton yield of per $E_{\rm c.m.}$ unit, and $dN_{\rm target}/dE$ refers to the energy dependent hydrogen atom number. As aforementioned, the effective target thickness was computed by the ^{13}N range difference between the maximum and the minimum energies of per $E_{\rm c.m.}$ unit in the $(CH_2)_n$. In addition, it was also checked by the Monte-Carlo simulation of the target depth versus $E_{\rm c.m.}$ where the scattering takes place. The divergence of the two methods for $dN_{\rm target}/dE$ was less than 1%. Finally, the averaged $d\sigma/d\Omega$ in the center of mass frame was obtained by

$$\left(\frac{d\sigma}{d\Omega}\right)_{\rm c.m.} = \frac{1}{4\cos\theta_{\rm lab}}\left(\frac{d\sigma}{d\Omega}\right)_{\rm lab}, \tag{4}$$

where $\theta_{\rm lab} = 15^\circ$.

B. *R*-matrix analysis

The sharp structures in the experimental proton spectrum are due to the formation of the compound nucleus ^{14}O, when the collision energies coincide with the specific excited states. The theoretical formalism to solve the resonant processes is the *R*-matrix theory. According to the model, the differential cross section can be written into a sum of pure Coulomb, resonant, and interference terms. The main assumption is that nuclear reactions (resonances) can take place only in the internal region defined by a channel radius of $a_c = r_0(m_t^{1/3} + m_p^{1/3})$, where m_t and m_p are the masses of the target and projectile, respectively. A comprehensive review of *R*-matrix theory can be found in Ref. [21].

The *R*-matrix $R_{c'c}$ is given by

$$R_{c'c} = \sum_\lambda \frac{\gamma_{\lambda c'}\gamma_{\lambda c}}{E_\lambda - E}, \tag{5}$$

where c and c' denote different channels and λ denotes the level index. The reduced widths $\gamma_{\lambda c}^2$ are related with the Coulomb penetrabilities $P(l)$ by

$$\gamma_{\lambda c}^2 = \Gamma_{\lambda c}/2P(l), \tag{6}$$

where $\gamma_{\lambda c}$ is the reduced width amplitude. The $P(l)$ are defined by

$$P(l) = kr\big/\left(F_l^2 + G_l^2\right)\big|_{a_c}, \tag{7}$$

where k is the wave number and F_l and G_l are the regular and irregular Coulomb functions, respectively.

The experimental excitation function was analyzed by using a multilevel, multichannel *R*-matrix code MULTI7 [22]. The used channel radius is 4.7 fm for $^{13}\mathrm{N} + p$ with $r_0 =$ 1.40 fm, which is found not sensitive to the fitting results upon small changes of r_0 to 1.20 fm. For the $E_{\rm c.m.}$ range in this work, $P(l)$ decrease rapidly as l increase and the reduced widths for $l + 2$ normally exceed the single-particle Wigner limit of $\gamma^2 \leqslant \hbar^2/\mu a_c^2$; $l + 2$ mixings were therefore neglected. The ground state of ^{13}N has a spin and parity of $1/2^-$ and the channel spin is of two values $s = 0^-$ or 1^- provided that only $^{13}\mathrm{N}_{\rm g.s}(J^\pi = 1/2^-)$ is taken into account; this is true for the observed ^{14}O levels below 7.0 MeV. For an observed resonance level, the main input parameters to the MULTI7 calculation include the resonance energy, width, and spin and parity; these parameters are manually changed until the best visual fit is achieved, while s and l are subject to the conservation laws. The normalization is done by comparing the area under the theoretical differential cross section to that under the data curve. The uncertainties of deduced E_R are given mainly based on the experimental resolution. In addition, another *R*-matrix code SAMMY-M6-BETA was also used to check the consistency of deduced results. Because SAMMY-M6-BETA allows for multilevel *R*-matrix fits to the experimental differential cross sections by solving Bayes's equations, it provides the fine tuning of the resonance parameters obtained by MULTI7 and gives the uncertainties for Γ_R as well.

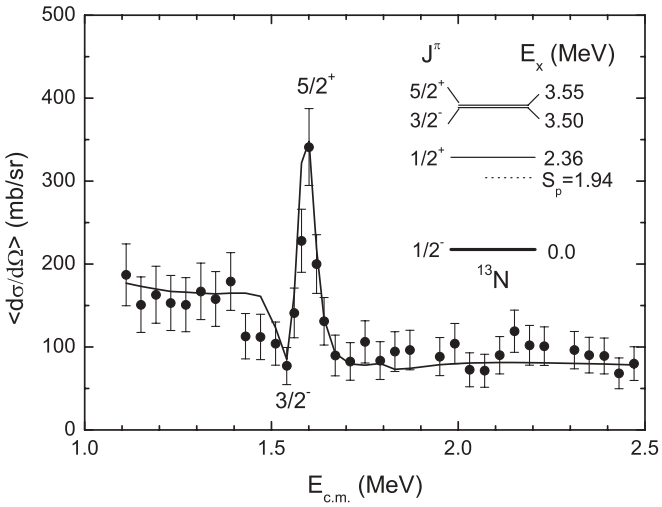

FIG. 4. A part of the excitation function from the scattering of $^{12}C + p$. The vertical scale is the averaged differential cross section. The solid line shows the fitting result as described in the text.

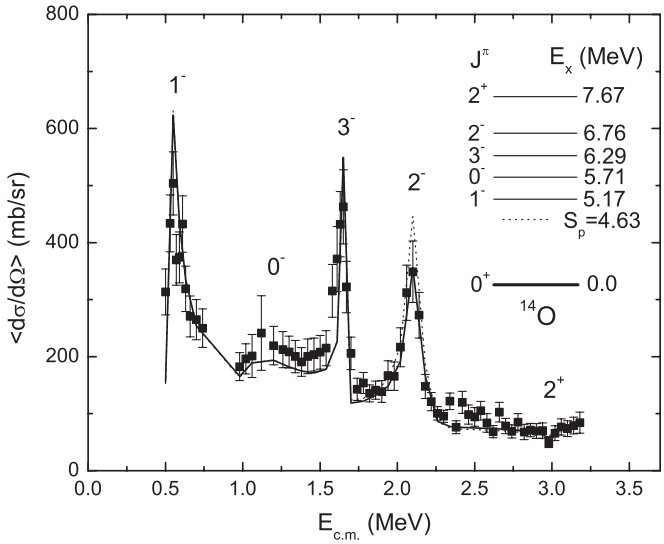

FIG. 5. The experimental excitation function for the $^{13}N + p$ scattering. The vertical scale is the averaged differential cross section. The solid line shows the fitting result at $\theta_{c.m.} = 150^\circ$. The dotted line represents a fitting calculation with only $s = 0$ for the 2^- state. The gaps at $E_{c.m.} = 0.8$ MeV are due to the detector dead layers.

C. Results

A part of the excitation function from the scattering of $^{12}C + p$ is shown in Fig. 4. The error bars indicate the statistical uncertainties only. The systematical errors including the uncertainties in the detector solid angle and beam normalization are small compared with the statistical ones. As one can see from Fig. 4, the $3/2^-$ and $5/2^+$ states in ^{13}N lying at 3.50 and 3.55 MeV, respectively, are discernible and well fitted with the calculation at $\theta_{c.m.} = 150^\circ$. The input widths of 62 and 47 keV, respectively, are from an evaluation published in Ref. [16]. In the fitting calculation, the width and spin parameters were fixed, only the experimental excitation function needed a shift of 9 keV ($E_{c.m.}$) downward to meet the known resonances; this was taken into account in processing the excitation function of $^{13}N + p$ scattering and also set a lower limit for the $E_{c.m.}$ uncertainty.

The experimental excitation function for the $^{13}N + p$ scattering is shown in Fig. 5. The presented errors include the statistical and systematical ones. The latter were mainly due to the uncertainties in the detector solid angle (4%) and in beam normalization (6%). The fitting calculations were done with MULTI7 and SAMMY-M6-BETA at $\theta_{c.m.} = 150^\circ$ with parameters listed in Table I.

IV. DISCUSSION

In general, our results agree with those published recently [8,17] (see Table I), particularly with Ref. [8] due to the similar method and setup adopted. Several selected resonance levels are briefly discussed in the following.

A. 5.17 MeV 1^- state

The 1^- state at 5.17 MeV in ^{14}O has been intensively studied before because of its significance for the $^{13}N(p,\gamma)^{14}O$ reaction rates [10–15]. The latest adopted resonance parameters are $E_R = 527.9 \pm 1.7$ keV, $\Gamma_p = 37.3 \pm 0.9$ keV, and $\Gamma_\gamma = 3.36 \pm 0.72$ eV [15]. The present work agrees with the adopted values of E_R and Γ_p within errors.

B. 5.71 MeV 0^- state

The systematics of $A = 14$ nuclides [16] indicate a 0^- level at 6.90 and 8.78 MeV in ^{14}C and ^{14}N, respectively. Prior to Ref. [8], the 0^- level in ^{14}O had never been observed. The $^{13}N + p$ entrance channel populates 1^- ($E_x = 5.17$ MeV) and

TABLE I. Resonance parameters deduced from the fitting calculation of the $^{13}N + p$ scattering.

		This work		Ref. [8]		Ref. [17]	
J^π	l	E_x (MeV)	Γ_R (keV)	E_x (MeV)	Γ_R (keV)	E_x (MeV)	Γ_R (keV)
1^-	0	5.169(19)	40(4)	5.159(10)	42(4)	5.178(10)	37(14)
0^-	0	5.710(20)	400(45)	5.710(20)	400(100)		
0^+						5.931(10)	<12
3^-	2	6.290(20)	25(3)	6.285(12)	42(2)	6.284(9)	50(6)
2_1^+						6.609(10)	<5
2^-	2	6.759(19)	105(10)	6.767(11)	90(5)	6.762(30)	107(40)
2_2^+	1	7.670(50)	62(10)	7.745(19)	63(16)	7.777(10)	77(9)

0^- states in ^{14}O via an s-wave resonance leading to a main configuration of the proton $1p_{1/2} \otimes 2s_{1/2}$ in the final stage, and is therefore sensitive to this missing unnatural parity state. It was indeed observed in Ref. [8] at 5.7 MeV with a width of 400(100) keV, the present work has confirmed the new 0^- level with a width of 400(45) keV.

C. 6.29 MeV 3^- state

The 6.29 MeV 3^- state in ^{14}O can be populated with the $^{13}\mathrm{N} + p$ system via a d-wave resonance leading to a main configuration of the proton $1p_{1/2} \otimes 1d_{5/2}$. The level has been established relatively well provided that only its E_R and J^π are considered [16]. The width value of 103(6) keV that entered into the compilation [16] is from an early study of the reaction ^{12}C(^{3}He,n)^{14}O(p)^{13}N [23]. The recent high-resolution study of the ^{14}N(^{3}He,t)^{14}O reaction determined a much smaller width of 50(6) keV [17]. The $^{13}\mathrm{N} + p$ resonance scattering in Ref. [8] gave a value of 42(2) keV. In the present work, an even smaller value of 25(3) keV was found suitable to fit the amplitude of the experimental peak.

D. 6.76 MeV 2^- state

Prior to the very recent work in Ref. [8], the 6.8 MeV level in ^{14}O was observed with only a certain assignment of negative parity [16]. Its width was determined with a large uncertainty of 107(40) keV in the cited work with the ^{14}N(^{3}He,t)^{14}O reaction [17]. A clear assignment of 2^- was made in Ref. [8] with a width of 90(5) keV based on an R-matrix analysis including only $s = 1$. In the present work, the spin assignment and the width value were confirmed. Because both $s = 0$ and 1 with $l = 2$ satisfy the conservation law, which means that a mixing of the proton $d_{3/2}$ and $d_{5/2}$ is probable, both channel spins were included in the fitting calculation. The results do not change much with pure $s = 1$ (solid line in Fig. 5) or with mixing up to 1:1, therefore the mixing ratio can not be uniquely determined if any. The pure $s = 0$ does not fit the data (dotted line in Fig. 5).

E. Other states

The population of 0^+ and 2^+ excited states in ^{14}O with $l = 1$ partial waves is suppressed at large $\theta_{\mathrm{c.m.}}$ angles. 0^+ and 2_1^+ levels at 5.9 and 6.6 MeV, respectively, did not directly show up in the experimental proton spectrum. According to Ref. [17], the widths of these two levels are minute with upper limits of 12 and 5 keV, respectively, which are much smaller than the present experimental resolution. These two levels were therefore not included in the fitting calculation. For the 7.7 MeV 2_2^+ level, the present work suffered from the difficulties in the discrimination of the proton events from electronic noises due to very small energy losses in the DSSSD. We note the near 100 keV difference of E_R from the compiled value, yet the present value of Γ_p is in agreement with the ones reported in recent works.

In summary, the excitation function for the $^{13}\mathrm{N} + p$ elastic resonance scattering has been measured in inverse kinematics via a novel thick-target method. The overall agreements with the results published shortly before enhance the confidence of the observation of the new 0^- level at 5.7 MeV and the assignment of 2^- to the state at 6.8 MeV in ^{14}O. R-matrix calculation indicates that the 6.8 MeV 2^- level may involve a mixing of $s = 0$ and $s = 1$ up to 1:1. Detailed measurements with intensive ^{13}N beam at more angles are necessary to clarify the nature of the 2^- states in ^{14}O and to remove the discrepancies of deduced resonance parameters, particularly for the 3^- level at 6.3 MeV.

ACKNOWLEDGMENTS

The authors thank Professor John Shriner of Tennessee Technological University for providing us with the multilevel R-matrix code MULTI7 and instructive communications. This work is supported by the National Natural Science Foundation of China under Grants 10445004 and 10575136 and Major State Basic Research Development Program under Contract 2007CB815003.

[1] S. Kubono, Nucl. Phys. **A693**, 221 (2001), and references therein.
[2] M. S. Smith and K. E. Rehm, Annu. Rev. Nucl. Part. Sci. **51**, 91 (2001), and references therein.
[3] C. Angulo, M. Azzouz, P. Descouvemont, G. Tabacaru, D. Baye, M. Cogneau, M. Couder, T. Davinson, A. Di Pietro, P. Figuera, M. Gaelens, P. Leleux, M. Loiselet, A. Ninane, F. de Oliveira Santos, R. G. Pizzone, G. Ryckewaert, N. de Séréville, and F. Vanderbist, Nucl. Phys. **A716**, 211 (2003).
[4] K. Markenroth, L. Axelsson, S. Baxter, M. J. G. Borge, C. Donzaud, S. Fayans, H. O. U. Fynbo, V. Z. Goldberg, S. Grévy, D. Guillemaud-Mueller, B. Jonson, K.-M. Källman, S. Leenhardt, M. Lewitowicz, T. Lönnroth, P. Manngård, I. Martel, A. C. Mueller, I. Mukha, T. Nilsson, G. Nyman, N. A. Orr, K. Riisager, G. V. Rogachev, M.-G. Saint-Laurent, I. N. Serikov, N. B. Shulgina, O. Sorlin, M. Steiner, O. Tengblad, M. Thoennessen, E. Tryggestad, W. H. Trzaska, F. Wenander, J. S. Winfield, and R. Wolski, Phys. Rev. C **62**, 034308 (2000).
[5] T. Teranishi, S. Kubono, S. Shimoura, M. Notani, Y. Yanagisawa, S. Michimasa, K. Ue, H. Iwasaki, M. Kurokawa, Y. Satou, T. Morikawa, A. Saito, H. Baba, J. H. Lee, C. S. Lee, Zs. Fülöp, and S. Kato, Phys. Lett. **B556**, 27 (2003).
[6] W. Galster, P. Leleux, I. Licot, E. Lienard, P. Lipnik, D. Mertens, T. Delbar, J. Vervier, P. Decrock, M. Huyse, P. Van Duppen, P. Duhamel, J. Vanhorenbeeck, G. Roters, C. Rolfs, U. Schroeder, H. P. Trautvetter, K. Wolke, J. Lambert, and W. S. Rodney, Phys. Rev. C **44**, 2776 (1991).
[7] J. Gómez del Campo, A. Galindo-Uribarri, J. R. Beene, C. J. Gross, J. F. Liang, M. L. Halbert, D. W. Stracener, D. Shapira, R. L. Varner, E. Chavez-Lomeli, and M. E. Ortiz, Phys. Rev. Lett. **86**, 43 (2001).
[8] T. Teranishi, S. Kubono, H. Yamaguchi, J. J. He, A. Saito, H. Fujikawa, G. Amadio, M. Niikura, S. Shimoura, Y. Wakabayashi, S. Nishimura, M. Nishimura, J. Y. Moon, C. S. Lee, A. Odahara, D. Sohler, L. H. Khiem, Z. H. Li, G. Lian, and W. P. Liu, Phys. Lett. **B650**, 129 (2007).

[9] C. Ruiz, T. Davinson, F. Sarazin, I. Roberts, A. Robinson, P. J. Woods, L. Buchmann, A. C. Shotter, P. Walden, N. M. Clarke, A. A. Chen, B. R. Fulton, D. Groombridge, J. Pearson, and A. S. Murphy, Phys. Rev. C **71**, 025802 (2005).

[10] P. Decrock, Th. Delbar, P. Duhamel, W. Galster, M. Huyse, P. Leleux, I. Licot, E. Liénard, P. Lipnik, M. Loiselet, C. Michotte, G. Ryckewaert, P. Van Duppen, J. Vanhorenbeeck, and J. Vervier, Phys. Rev. Lett. **67**, 808 (1991).

[11] P. Decrock, Th. Delbar, W. Galster, M. Huyse, P. Leleux, I. Licot, E. Liénard, P. Lipnik, C. Michotte, P. Van Duppen, J. Vanhorenbeeck, and J. Vervier, Phys. Lett. **B304**, 50 (1993).

[12] M. S. Smith, P. V. Magnus, K. I. Hahn, R. M. Curley, P. D. Parker, T. F. Wang, K. E. Rehm, P. B. Fernandez, S. J. Sanders, A. García, and E. G. Adelberger, Phys. Rev. C **47**, 2740 (1993).

[13] P. V. Magnus, E. G. Adelberger, and A. Garcia, Phys. Rev. C **49**, R1755 (1994).

[14] Xiaodong Tang, A. Azhari, Changbo Fu, C. A. Gagliardi, A. M. Mukhamedzhanov, F. Pirlepesov, L. Trache, R. E. Tribble, V. Burjan, V. Kroha, F. Carstoiu, and B. F. Irgaziev, Phys. Rev. C **69**, 055807 (2004).

[15] Z. H. Li, B. Guo, S. Q. Yan, G. Lian, X. X. Bai, Y. B. Wang, S. Zeng, J. Su, B. X. Wang, W. P. Liu, N. C. Shu, Y. S. Chen, H. W. Chang, and L. Y. Jiang, Phys. Rev. C **74**, 035801 (2006).

[16] F. Ajzenberg-Selove, Nucl. Phys. **A523**, 1 (1991).

[17] A. Negret, T. Adachi, G. P. A. Berg, P. von Brentano, H. Fraiquin, D. De Frenne, H. Fujita, K. Fujita, Y. Fujita, K. Hatanaka, E. Jacobs, K. Nakanishi, L. Popescu, Y. Sakemi, Y. Shimbara, Y. Shimizu, Y. Tameshige, A. Tamii, M. Uchida, and M. Yosoi, Phys. Rev. C **71**, 047303 (2005).

[18] X. Bai, W. liu, J. Qin, Z. Li, S. Zhou, A. Li, Y. Wang, Y. Cheng, and W. Zhao, Nucl. Phys. **A588**, 273c (1995).

[19] W. P. Liu, Z. H. Li, X. X. Bai, Y. B. Wang, G. Lian, S. Zeng, S. Q. Yan, B. X. Wang, Z. X. Zhao, T. J. Zhang, H. Q. Tang, B. F. Yang, X. L. Guan, and B. Q. Cui, Nucl. Instrum. Methods Phys. Res. B **204**, 62 (2003).

[20] Micron Semiconductor, Lancing, Sussex, UK, http://www.micronsemiconductor.co.uk/.

[21] A. M. Lane and R. G. Thomas, Rev. Mod. Phys. **30**, 257 (1958).

[22] R. O. Nelson, E. G. Bilpuch, and G. E. Mitchell, Nucl. Instrum. Methods Phys. Res. A **236**, 128 (1985).

[23] J. G. Pronko, R. G. Hirko, and D. C. Slater, Phys. Rev. C **7**, 1382 (1973).